Energy, Environmental, and Catalysis Applications

Design of monolithic supports by 3D printing for its application in the preferential oxidation of CO (CO-PrOx)

Cristian Yesid Chaparro Garnica, Esther Bailon-Garcia, Arantxa Davó-Quiñonero, Dolores Lozano-Castello, and Agustín Bueno-López

ACS Appl. Mater. Interfaces, **Just Accepted Manuscript** • DOI: 10.1021/acsami.9b12731 • Publication Date (Web): 19 Sep 2019

Design of monolithic supports by 3D printing for its application in the preferential oxidation of CO (CO-PrOx)

Cristian Yesid Chaparro-Garnica, Arantxa Davó-Quiñonero, Esther Bailón-García, Dolores Lozano-Castelló, Agustín Bueno-López.*

Department of Inorganic Chemistry, University of Alicante, Carretera de San Vicente s/n, E03080, Alicante (Spain).

KEYWORDS: 3D printing; CO-PrOx; monolith; ceria; preferential oxidation

Corresponding author: E. Bailón-García
E-mail: estherbg@ugr.es

Abstract

Honeycomb-shaped cordierite monoliths are widely used as supports for a great number of industrial applications. However, the high manufacturing costs of cordierite monoliths only justifies its use for high temperatures and aggressive chemical environments, demanding applications where the economic benefit obtained exceeds the manufacturing costs. For low demanding applications, such as the preferential oxidation of CO (CO-PrOx), alternative materials can be proposed in order to reduce manufacturing costs. Polymeric monoliths would be an interesting low-cost alternative, however, the handicap of the active phases incorporation to the polymeric support must be overcome. In this work, the implementation and use of polymeric monolithic structures obtained by 3D-printing to support CuO/CeO_2 catalysts for CO-PrOx has been studied. Several approaches were used to anchoring the active phase into the polymeric monoliths, such as adding inorganic materials (carbon or silica) to the polymer previous to the printing process, chemical attack with solvents of the printed resin previous or during the active phase incorporation, perform consecutives impregnations and modification of the channel walls design. Among those approaches, best results were obtained by the addition of silica and by the channel modification. Independently of the strategy followed, a subsequent thermal treatment in N_2 was required to soften the resin and favor the active phase anchoring. However, catalyst particles become embedded on the polymeric resin being not active and thus, a final cleaning thermal treatment under air was needed to recover the active phase activity, after which the supported active phase demonstrated good catalytic activity, stability and reusability.

1. Introduction

The burn of fossil fuels such as oil, coal and natural gas has been the main energy sources used to meet the energy requirement of the industry and society.[1,2] However, the increasingly scarce reserve of fossil fuels and the environmental problems derived from its combustion have motivated the search of cleaner and renewable energetic systems. Hydrogen has been proposed as an alternative energetic vector to replace fossil fuels, either through combustion or by direct conversion of its chemical energy into electrical energy by electrochemical reactions. However, some limitations must be overcome in terms of production, storage and distribution for a real implementation of the hydrogen economy.[3]

Fuel cells technology is the most promising alternative to combustion engines for stationery and transport uses since they are potentially more efficient than heat engines because of fuel cells are not limited by the Carnot cycle efficiency, and they are a clean technology which generates water as the only by-product. Of all the fuel cells, proton exchange membrane fuel cells (PEMFCs) is gaining most of the attention in automotive applications. PEMFCs are popular due to their relatively low operating temperature and high efficiency. However, the PEMFC operates by using platinum-coated membranes as a catalyst and thus, a high pure hydrogen feed is required to avoid the catalyst poisoning. Most of the H_2 produced to date has been obtained from fossil fuels, being the steam reforming (SR) of hydrocarbons one of the most used H_2 production processes, leading to a significant co-production of CO_2[4] which must be captured for their subsequent transformation, guaranteeing an environmentally sustainable process.[5] Moreover, the obtained mixture of H_2 is accompanied by 10-15% of CO which has to be removed to, as commented, avoid the electrocatalyst (Pt/C) poisoning. To reach the established tolerance levels of CO to ensure the correct operation of the PEMFC catalysts, it is necessary to

carry out several stages after the SR.[6–10] One of these stages is the water gas-shift reaction (WGS), after which 0.5 to 1.0 vol % of unconverted CO still remains in the effluent with which the performance of the PEMFCs is still affected by the preferred chemisorption of the CO over the Pt.[11] For this reason, before feeding the fuel cell, an additional stage must be incorporated to reduce the CO concentration to values below 10 ppm.

To achieve this aim, great interest has been focused on the CO preferential oxidation (CO-PrOx) reaction, seeking selectivity to the oxidation of the minor component of the gas stream (CO) against the major one (H_2), since the two components are susceptible to oxidation. For this, catalysts must be developed to adjust to the demands of the process, where the reactions involved are the following:

$$CO + ½O_2 \leftrightarrow CO_2 \qquad \Delta H^{\circ}_{25^{\circ}C} = -283 \text{ KJ/mol}$$

$$H_2 + ½O_2 \leftrightarrow H_2O \qquad \Delta H^{\circ}_{25^{\circ}C} = -242 \text{ KJ/mol}$$

In addition, other reactions such as the WGS, the inverse WGS and the methanation of CO or CO_2 can occurs, which affect the efficiency of the process.[12] For this reason, the catalysts used in the CO-PrOx reaction must have high activity to the oxidation of CO, be selective to the CO oxidation with respect to the H_2 oxidation reaction, have resistance to the deactivation by H_2O and CO_2 and be operational in the typical temperature range of the PEMFCs (<250 ºC).

The good catalytic behavior of CuO/CeO_2, and the great advances in its optimization for the CO-PrOx reaction, have led it to be among the most used and studied catalysts to purify the hydrogen supply for PEM fuel cells.[13] However, these catalysts have been mainly used in compact bed reactors with randomly packed catalyst particulates which have large volumes, high pressure drop and a slow response to transient operations necessary for a load-following fuel cell system and are subject to attrition.[14] In addition,

the PEMFCs are mainly conceived to be favorable alternatives to conventional electricity generation methods for small-scale applications as required for electric vehicles and residential power generators,[15] thus the use of compact bed reactors is limited since its application at small-scale is difficult.[12,16]

The monolithic supports can be a better option to replace the compact bed reactors in the CO-PrOx reaction for applications in PEM fuel cells. Monolith reactors can have much smaller volumes than packed beds, are more robust than powdered catalysts, are structurally stable against mechanical attrition or washcoat loss, have greater resistance to frictional wear, have good heat and mass transfer characteristics and, furthermore, they offer little pressure drop, and have rapid response to transient modes of operation.[12,16,17] Moreover, they are easily manipulated for installation or replacement, and unlike fixed-bed reactors, prevent the formation of preferred paths when circulating gas streams.[18–21] Barbato *et al.*[12] evidenced that the use of structured catalysts allows to overcome the limitations of intra-particle mass transfer that generally occur in powder catalysts at high conversions, improving the use of active phases. Consequently, monolithic reactors are preferred against packed fixed-bed reactors for industrial applications.

Honeycomb-shaped ceramic monoliths are the commonly used monolithic supports of active phases. Cordierite is the standard material to produce the honeycomb monoliths, however, manufacturing of cordierite monoliths is inherently costly since they are mainly manufactured by extrusion and high temperatures are required to sinter and crystallize glass powders cordierite.[22,23] Thus, the use of these supports is only justified for high demanding applications involving high temperatures and aggressive chemical environments, when the economic benefit obtained exceeds the high manufacturing costs.[22] However, the temperature required for CO-PrOx reaction is lower than 250 ºC, thus, cheaper alternative materials can be considered. Polymeric monoliths can be an

interesting alternative to cordierite in low-temperature applications since they can be easily produced at low cost. The use of 3D-printing technology for the design of monoliths with specific configurations would be a breakthrough in the field of catalysis. It should be noted that 3D-printing is being successfully used in many fields of medicine, architecture or engineering, but has rarely been used in the area of heterogeneous catalysis. However, the applicability of 3D printed polymeric monoliths is limited by its thermal and chemical stability, together with the difficulty to incorporate the active phases to the polymeric support. Thus, the first handicap that must be overcome to do of the 3D impression of specified designed catalytic supports a reality, is the incorporation of active phases to polymers.

In this context, the present work focuses on the implementation and use of polymeric monolithic structures obtained by 3D-printing to support CuO/CeO_2 catalysts used in the preferential oxidation of CO (CO-PrOx), as an alternative to design and manufacture monolithic supports with complex geometries that allow improving the performance of the catalysts currently used. Especial attention has been paid to the incorporation of the active phase to these polymeric monoliths, the main drawback of this traditional 3D-printing technology.

2. Experimental Section

2.1. Catalyst Preparation

3D-printed Monoliths

The monoliths were prepared by 3D-printing using a photosensitive liquid resin VisiJet® FTX Green supplied by 3D Systems. The liquid resin was doped with different amounts of carbon (Vulcan XC72) or SiO_2 (Silica Fumed S5130) to study its influence on the subsequent active phase anchoring and on the thermal stability of the obtained polymeric

monoliths. The samples were identified according to the weight percentage of C and SiO_2 incorporated to the resin, e.g. 0.13 % C or 0.35 % SiO_2. The honeycomb polymeric monoliths (cylinder: Ø=10mm, L=15mm) were printed with two different designs in the channels in order to favor the anchoring of the active phase. The weight of all monoliths printed was 1.1 ± 0.1 grams and channels had a square section with 0.1 x 0.1 cm. The first design was a conventional honeycomb monolith (called conventional design, CD) in which channels had completely flat walls, while the second design was an advanced monolith (called advanced design, AD) which had 15 prismatic cavities along the walls of each channel. This second design was proposed to improve the anchoring of the powdered catalyst to the monolithic support. A photograph of the AD monolith is shown in **Figure 1a** and a schematic representation of the prismatic cavities depicted in **Figure 1b**.

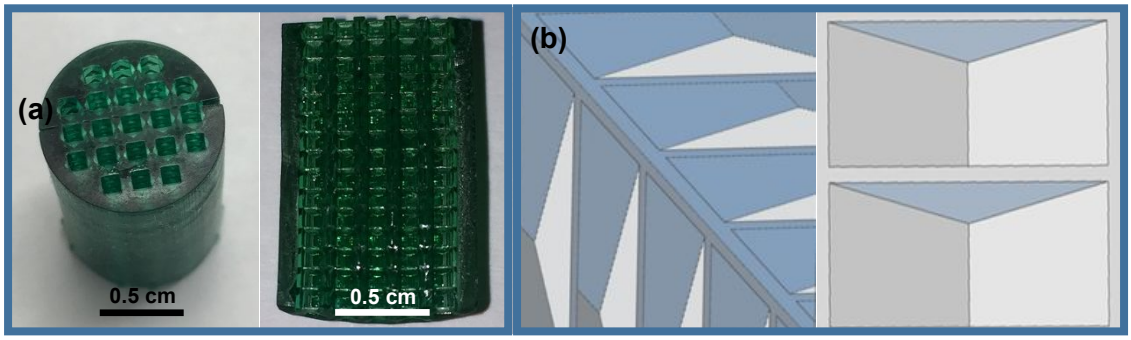

Figure 1. Monolith obtained by 3D-printing. (a) Photograph of channel-modified monolith (AD) and (b) schematic representation of the prismatic cavities along the walls of each channel of an AD monolith.

Active phase synthesis

The synthesis of the CuO/CeO_2 active phase was the second stage of the preparation of the supported catalysts. Firstly, CeO_2 support was obtained by calcining $Ce(NO_3)_3 \cdot 6H_2O$ (99.5%, Alfa Aesar) in a muffle at 500 °C for 4 h using a heating rate of

5°C/min. The preparation of the CuO/CeO_2 catalyst was carried out by incipient wetness impregnation of the CeO_2 support with a solution of $Cu(NO_3)_2 \cdot 2.5H_2O$ (≥98%, Sigma-Aldrich) in distilled water. The amount of CuO precursor salt dissolved was calculated considering a final amount of 5 % by weight (w/w) of metallic Cu in the catalyst. After impregnation, the material was subjected to a flash dry by being introduced directly to a preheated muffle at 200°C. Finally, the temperature was increased at 2 °C/min up to 400 °C, holding at this temperature for 2 hours to decompose the CuO precursor salt and to obtain the final CuO/CeO_2 active phase.

Active-phase loading into the 3D-printed monoliths

To complete the preparation of the supported catalysts, the CuO/CeO_2 active phase was deposited on the monoliths by dip-coating. Different strategies were used in order to improve the active phase anchoring: i) attack of the resin with ethanol or isopropanol previous to the dip-coating process by dipping once the monolith into a pure ethanol or isopropanol solution, ii) attack of the resin during the dip-coating process by using ethanol or isopropanol as solvent of the catalysts suspension and iii) perform two consecutive impregnations.

Briefly in a typical dip-coting process, suspensions of 10 g/ml of CuO/CeO_2 catalysts were prepared. Water, isopropanol and ethanol were used as liquid phases in order to analyze the effect of the solvent attach to the polymeric resin on the anchoring capacity. Both monoliths were dipped twice into this suspension (once each side drying the monoliths in between). The samples were dried at room temperature for 24 hours and after that, were submitted to a stabilization thermal program in an N_2 atmosphere (100 ml/min) consisting in a step at 150 ºC for 2 hours at a heating rate of 5 °C/min, and then at 250 ºC for 2 h at a heating rate of 2.5 °C/min. Catalysts were referred as the active phase followed by the monoliths name and finally the treatment atmosphere, e.g.

CuO/CeO_2-AD (N_2) means that CuO/CeO_2 active phase was deposited on the AD monolith and finally, treated only in N_2. In some cases, an additional oxidation thermal treatment was also carried out in static air at 250 ºC for 2 hours at a heating rate of 2.5 °C/min using a muffle. In this case the catalysts were referred following the same nomenclature system but identifying the air atmosphere, e.g. CuO/CeO_2-AD (air)

2.2. Catalyst characterization

The thermal stability of the resins was determined by thermogravimetric analysis in an SDT 2960 analysis equipment, Simultaneous DSC-TGA, TA Instruments.

The amount of active phase anchored in the monoliths was determined by gravimetric measurements taking into account the weight loss percentage that the polymeric resin suffers after the stabilization thermal treatments as well as by burning the polymeric resin at 550 ºC for 2 h, obtaining comparable results with less than 2 % of error.

The surface area of the powder catalyst was measured by N_2 isotherms at -196 ºC using a Quantachrome Autosorb-6B equipment after degassing the samples at 250 ºC for 4 h.

The elemental composition of the powder sample was confirmed by micro x-ray fluorescence (μXRF) in an Orbis Micro-XRF Analyzer by EDAX.

The crystalline species of the samples were identified by x-ray diffraction (XRD) using a Rigaku Miniflex II diffractometer, employing a Cu Kα radiation ($\lambda = 0.15418$ nm).

The Raman spectra of the powdered and supported catalysts were obtained with a dispersive Raman spectrometer model Bruker RFS/100 with coupled microscope.

The surface chemistry was analyzed by X-ray photoelectron spectroscopy (XPS) in a K-ALPHA Thermo Scientific device, using Al-Kα radiation (1486.6 eV). The X-ray spot was focused on the catalysts with a diameter of 400 μm, at 3 mA × 12 kV. The binding energy scale was adjusted by setting the C1s transition at 284.6 eV.

The characterization of morphology and chemical analysis of the CuO/CeO_2 supported catalysts in polymer resin monoliths was carried out by scanning electron microscopy (SEM) in a HITACHI S-3000N microscope with an XFlash 3001 X-ray detector by Bruker for microanalysis (EDS) and chemical mapping.

2.3. Catalytic Tests

Catalytic tests were carried out using the powdered and 3D-printed monolith-supported catalysts. In all the tests (powdered and supported catalysts) the amount of active phase available in the reactors was controlled, allowing the results to be comparable. The catalytic experiments were carried out in a stainless-steel cylindrical reactor coupled to a gas chromatograph (Agilent Technologies 6890N) equipped with two columns: Porapak Q 80/100 for CO_2 and H_2O separation and Molecular Sieve 13X for O_2 and CO separation.

The gas mixture fed to the reactor was adjusted in 2% CO, 2% O_2 and 30% H_2 with He balance. Total flows of 30, 60, 90 and 120 ml/min were fixed with mass flow controllers (MFCs Bronkhorst).

In a typical experiment, the reaction gas mixture was fed to the reactor at room temperature for 30 min, and then the temperature was raised at 2 °C/min until 250 °C. Then, the reaction gas mixture was replaced by 5% O in He, keeping this flow during cooling. After 15 min at 250 °C the furnace was switched of and the reactor was cooled down without control of the cooling rate. Following this protocol, several consecutive experiments were performed to study the reproducibility of the catalytic results.

The CO conversion and selectivity to CO oxidation were calculated according to the following equations.

$$\text{CO conversion (\%)} = \frac{[\text{CO}]\text{in} - [\text{CO}]\text{out}}{[\text{CO}]\text{in}} \cdot 100$$

$$\text{CO selectivity (\%)} = \frac{[\text{CO}]\text{in} - [\text{CO}]\text{out}}{[\text{O}_2]\text{in} - [\text{O}_2]\text{out}} \cdot \frac{1}{2} \cdot 100$$

3. Results and discussion

3.1. Catalysts characterization

Thermal stability of the 3D-printed polymeric monoliths

The first important thing to study when designing polymer monoliths for catalysis is the thermal stability of such polymeric monoliths in order to determine the operational temperature range. Thus, thermogravimetric analysis (TGA) under N_2 atmosphere was carried out to the 3D-printed monoliths. Monoliths obtained from pure resin as well as from different resin compositions (resin and carbon or silica) were printed and tested to analyze the thermal stability as well as the improvement obtained by the addition of inorganic materials, such as carbon or silica, to the resin composition. TGA plots are depicted in **Figure 2**. Note that all monoliths present a weight loss of around 8 % in the temperature range from 130 ºC to 200 ºC attributed to the removal of volatile substances present in the polymeric resin. Above 200 ºC, the monoliths are stable up to around 330 ºC where a strong weight loss occurs which is indicative of the resin degradation. It is important to bear in mind that this method of analysis provides information associated with the weight changes, so it does not allow knowing the chemical composition of the resin, or changes in crystallization or glass transition. However, the TGA profiles confirms that all the prepared monolithic supports can be used in the operate temperature range of the PEM fuel cells (<250 ºC).[6] It is also important to highlight that no important changes are observed in the thermal stability of the resin by the adition of inorganic materials such as carbon or SiO_2.

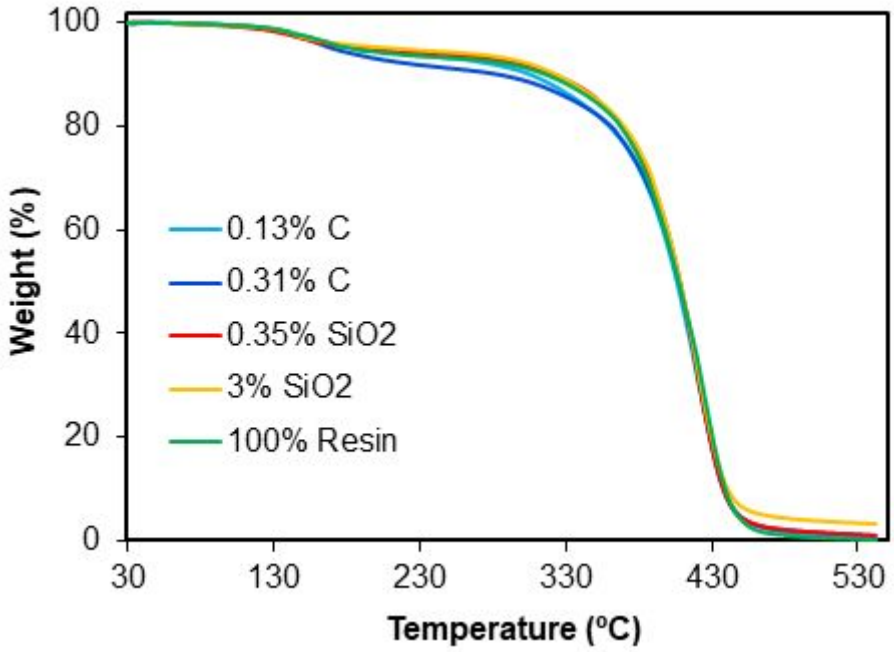

Figure 2. TGA of the different compositions of polymer resin, inert atmosphere (N_2)

In order to stabilize the polymeric 3D-printed monoliths in the operation temperature range of the PEMFC, they were subjected to a thermal stabilization treatment under N_2 atmosphere at 250 ºC for 1 hour and after that, the thermal stability under N_2 and O_2 atmospheres was again studied by TGA. Results are depicted in **Figure 3a** and **b**, respectively. It is indeed observed that after the previous treatment, the resin stabilizes, and no weight loss occurs in the monoliths until temperatures above 300ºC in both oxidizing and reducing atmosphere. This manifests that the 3D-printed monoliths can be used in application in which temperatures lower than 300 ºC are required as in the case of the CO-PrOx reaction.

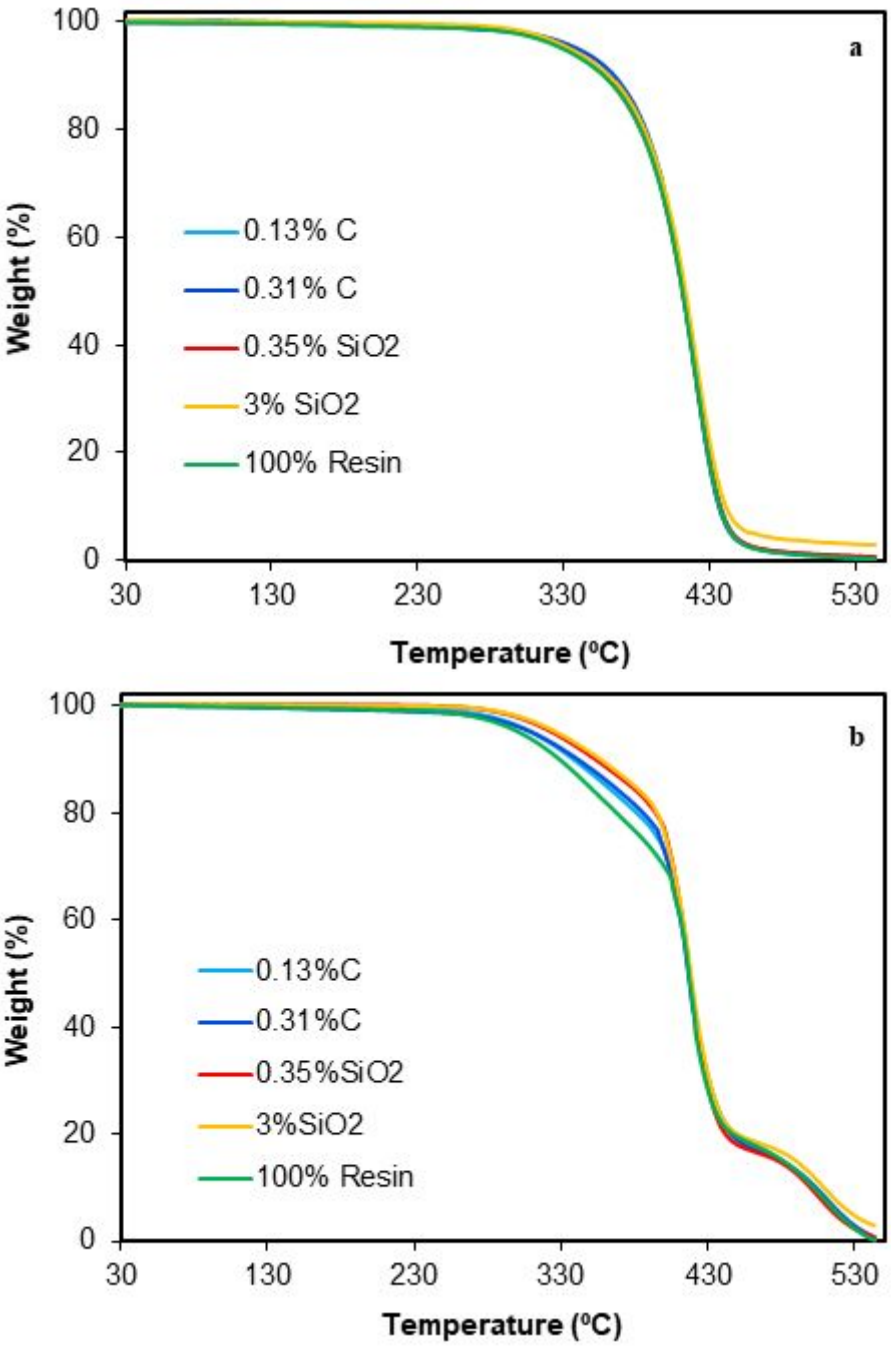

Figure 3. TGA of the monoliths performed under (a) N_2 atmosphere and (b) air after the stabilization treatment (stabilization was carried out in N_2 at 250ºC).

Incorporation of the active phase in the 3D-printed monoliths

Once knowing the thermal stability of the resin, the next step is the incorporation of the active phase to the 3D-printed monoliths. As it was commented in the experimental section, several strategies have been studied in order to favor the active phase

incorporation in the polymeric monoliths. In a first stage, the monolithic supports prepared from the different resin compositions were tested carrying out different impregnation methodologies such as the chemical attack with isopropanol or ethanol on the channels of the monoliths just before dip-coating, or the preparation of the catalyst suspensions with different dispersing media (water, isopropanol or ethanol). Initially, monoliths with conventional design (CD) were used and the amount of catalyst anchored by each strategy is presented in **Table 1**.

Table 1. Amount of CuO/CeO_2 anchored on the CD (conventional design) monolith after the thermal stabilization treatment in N_2 following the different impregnation procedures.

Resin composition	Design	Previous chemical attack	CuO/CeO_2 Suspension	CuO/CeO_2 anchored [mg]
Pure Resin	**CD**	**No**	**H_2O**	**31.6±0.9**
Pure Resin	CD	Isopropanol	H_2O	7.0±0.2
Pure Resin	CD	Ethanol	H_2O	6.0±0.2
Pure Resin	CD	No	Isopropanol	10.0±0.3
Pure Resin	CD	No	Ethanol	9.4±0.3
0.13% C	CD	No	H_2O	23.8±0.7
0.31% C	CD	No	H_2O	37.8±1.1
0.35% SiO_2	**CD**	**No**	**H_2O**	**51.6±1.4**
3% SiO_2	CD	No	H_2O	41.7±1.2

From the data collected in **Table 1**, it is observed that the chemical attack of the resin with ethanol or isopropanol either before or during the dip-coating process hinders the active phase incorporation to the monoliths achieving to anchor only around 7-10 mg regarding the 31.6 mg incorporated without chemical attack. Considering this optimal impregnation conditions (no chemical attack and water as dispersant of the CuO/CeO_2 catalysts), the effect of the addition of inorganic component to the resin composition was analyzed. Note that more amount of SiO_2 (3%) regarding carbon (0.31%) could be

incorporated to the resin composition without phase precipitation, which can be attributed to the smaller particle size of fumed silica (20-30 nm) regarding Vulcan carbon (50-100 nm) and to different chemical interactions with the resin. The incorporation of both inorganic materials improves the anchoring capacity of the polymeric monolith, but the improvement obtained with silica is higher than the obtained with carbon even at similar compositions (0.31 % of C and 0.35 % of SiO_2). The introduction of inorganic materials modifies the chemistry and rugosity of the resin surface creating anchoring points that favors the interaction with the active phase. The polymeric monolith doped with 0.35% SiO_2 (w/w) impregnated with a water suspension of CuO/CeO_2, is able to retain the greatest amount of active phase (51.6 mg). However, under the same conditions of impregnation, the monolithic support of pure resin is able to retain a significant amount of catalyst (31.6 mg), with the advantage of requiring fewer stages in its manufacturing process.

These two best resin compositions were selected (pure resin and resin with 0.35% of SiO_2) and monolithic supports were made with the advanced design, AD (**Figure 1**). The impregnation of these samples was carried out following the same procedure used in the conventional design (CD). Additionally, the anchoring capacity was tested after applying more than one impregnation step. These results are collected in **Table 2**. It was also pointed out that the best dispersant medium for preparing the catalyst suspension is water, and that chemical attacks on the resin do not improve the anchoring capacity of the monoliths. In addition, the monoliths with advanced design (AD) have greater anchoring capacity of CuO/CeO_2 in comparison with the monoliths of conventional design (CD), being this effect more noticeable in the monoliths obtained from pure resin (31.6 mg vs 51.2 mg for CD and AD, respectively). Taking into account that the addition of dopants into the resin does not provide appreciable improvement in thermal stability and that, as

shown by the results of **Table 2**, the modification of the design of the monolith allows to retain quantities similar to those retained by the doped monoliths, the advanced design of pure resin monoliths is selected as an efficient and interesting option to anchor active phases in polymeric monoliths avoiding the additional step of the resin doping with the difficulties that this implies in the impression process, e.g. dopant additions can hinder the printing of the monoliths if the resin is not mixed homogeneously.

Table 2. Amount of CuO/CeO_2 anchored in the monoliths after the thermal stabilization treatment in N_2 depending on the design (conventional design-CD and advanced design-AD) and the impregnation process.

Resin composition	Design	Previous chemical attack	CuO/CeO_2 Suspension	CuO/CeO_2 anchored [mg]
Pure Resin	CD	No	H_2O	31.6±0.9
0.35% SiO_2	CD	No	H_2O	51.6±1.4
Pure Resin	**AD**	**No**	**H_2O**	**51.2±1.4**
0.35% SiO_2	AD	No	H_2O	58.5±1.7
Pure Resin	AD	No	Isopropanol	17.3±0.5
Pure Resin	AD	No	Ethanol	12.1±0.4
Pure Resin	AD	Isopropanol	H_2O	25.3±0.8
Pure Resin	AD	Isopropanol	H_2O	32.7±0.9
Pure Resin*	AD	No	H_2O	55.7±1.7
Pure Resin **	AD	No	H_2O	61.1±1.7

* Sample with two stages of impregnation with 24 hours drying at room temperature between impregnations.
** Sample with two stages of impregnation with drying at room temperature for 24 hours and subsequent thermal treatment at 250ºC between impregnations.

With the aim to increase the amount of active phase incorporated into the AD polymeric monolith, two successive impregnations were performed making or not thermal stabilization treatment between each impregnation step (**Table 2**). It is observed that the amount of catalyst anchored to the monolith after two impregnation cycles is higher compared to the samples impregnated in a single stage. Note also, that the

stabilization treatment is required for the anchoring of the active phase as denotes the higher amount of the active phase incorporated after the second impregnation step after a first stabilization treatment (51.2 for one impregnation vs 55.7 and 61.1 mg for untreated and treated monoliths after a second impregnation, respectively). Nonetheless, this increase is not significant enough to justify the longer time and the additional required stages. As mentioned, the best results were given for the advanced-designed monolith (AD) printed from pure resin and thus, this catalyst was selected for characterization and catalytic tests.

Characterization of the CuO/CeO_2 active phase

X-ray fluorescence (μFRX) was carried out to the powdered active phase to confirm that the desired amount of Cu was deposited on the CeO_2 surface. **Table 3** shows the composition of the powdered active phase corroborating that 4.8 % by weight of Cu was effectively loaded on the CeO_2 support, which is very close to the theoretical desired value (5 %).

Textural properties of powdered ceria support and CuO/CeO_2 catalyst were analyzed by N_2 adsorption-desorption isotherms at -196 ºC and results are collected in **Figure 4** and **Table 3.** The specific surface area (S_{BET}) and micropores volume (V_{micro}) was determined by applying the Brunauer-Emmett-Teller and Dubinin-Radushkevich equations, respectively, to the N_2-isotherm. The total pore volume (V_{total}) was considered as the volume of N_2 adsorbed at $P/P_0 = 0.95$ and the mesopore volume (V_{meso}) was obtained by the difference between V_{total} and V_{micro}. Both support and catalyst present a type IV isotherm according to the IUPAC classification, corresponding to mesoporous solids. Those isotherms are characterized by a low N_2 uptake at low relative pressures denoting a low micropore volume (V_{micro}) and an increase of the N_2 uptake at medium relative pressures with a hysteresis loop indicative of the presence of mesopores. Note

that the hysteresis loop closes at high relative pressures, which indicates the presence of wide mesopores, probably created by the gas release during the calcination process. The hysteresis loop obtained in both cases is a H2 type one which can be attributed either to pore-blocking/percolation in a narrow range of pore necks or to cavitation-induced evaporation.[24] The fall of the desorption branch until close is not very abrupt, which indicates that despite bottle-ink type of pores are presented, the size distribution of neck widths is large.

Table 3. Specific surface area (B.E.T.) and X-ray micro-fluorescence (μFRX) of CeO_2 and CuO/CeO_2 powdered samples.

Sample	N_2-isotherm				μFRX
	S_{BET} ($m^2\ g^{-1}$)	V_{total} ($cm^3\ g^{-1}$)	V_{micro} ($cm^3\ g^{-1}$)	V_{meso} ($cm^3\ g^{-1}$)	Cu (wt. %)
CeO_2	78	0.21	0.04	0.17	-
CuO/CeO_2	69	0.18	0.04	0.14	4.8

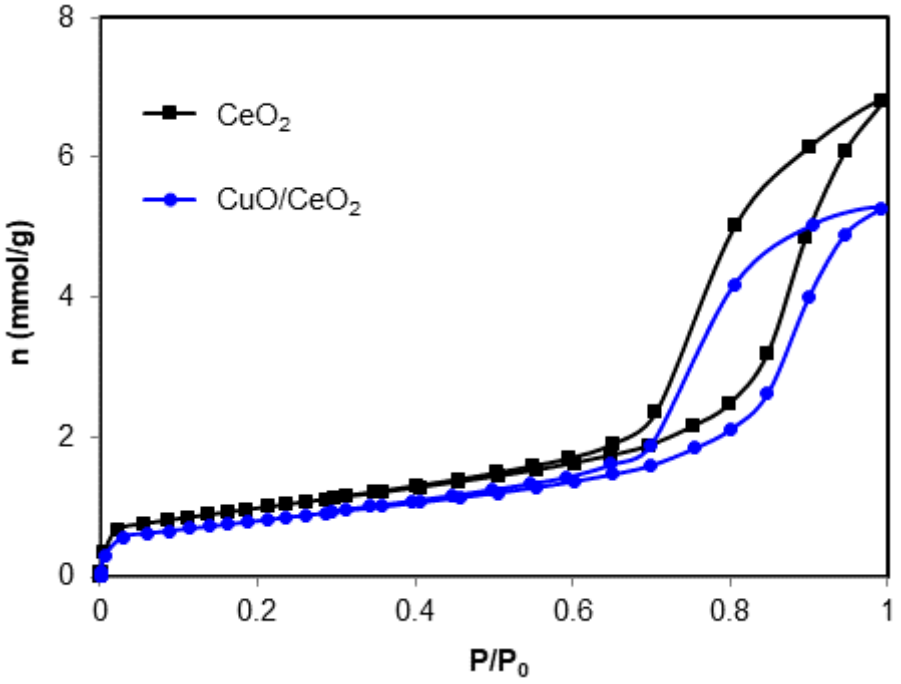

Figure 4. N_2 adsorption-desorption isotherms at -196ºC of CeO_2 and CuO/CeO_2 powdered catalyst

The deposition of CuO on the CeO_2 surface produces a mesopores blockage as denotes the lower V_{meso} and S_{BET} obtained for CuO/CeO_2 regarding CeO_2. This denotes that copper oxide particles are dispersed on the support surface occupying part of the porosity of the material.

The distribution of the active phase along the channels walls of the polymeric 3D-printed AD monolith was studied by SEM. **Figure 5a** and **d** show that the CuO/CeO_2 active phase is deposited along the channels of the monoliths but after the N_2 treatment, most of the catalyst particles seem to be embedded on the polymeric resin caused by the resin softening during the thermal treatment in N_2 or by the deposition of volatile substances on the catalyst surface during said treatment. This manifests that the thermal treatment of the monoliths under N_2 atmosphere after the impregnation step is not only required for the thermal stabilization of the resin but also is needed to favor the active phase anchoring corroborating the observation obtained analyzing the catalyst amount anchored after successive impregnation cycles. However, this active phase is not accessible to the reactant and a loss of activity can be expected. In order to improve the active phase accessibility, a cleaning treatment of the monolith surface was performed by a thermal treatment under air atmosphere. SEM images of such air-treated monoliths are depicted in **Figure 5c** and **d**. During this oxidizing thermal treatment, part of the resin that embed or cover the active phase is removed making it accessible as it is observed from **Figure 5**.

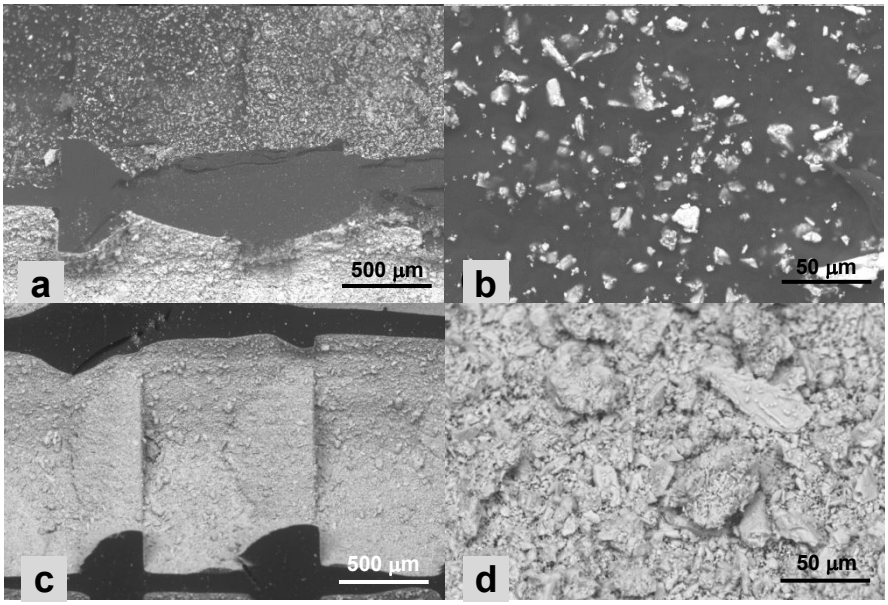

Figure 5. SEM images of the channels of AD monolith after the thermal stabilization treatment in N_2 (a and b) and after a subsequent thermal treatment in air (c and d).

A cross section SEM image of the air-treated monolith is collected in **Figure 6.** It is observed that the CuO/CeO_2 catalyst layer is covering the channel walls. In addition, it is verified that the contraction of the monoliths after the thermal treatment is almost negligible, and the dimensions of the channels (0.1 cm x 0.1 cm, approximately) are conserved after the thermal treatments. Small cracks corresponding to the elimination of volatile substances from the resin can be also observed.

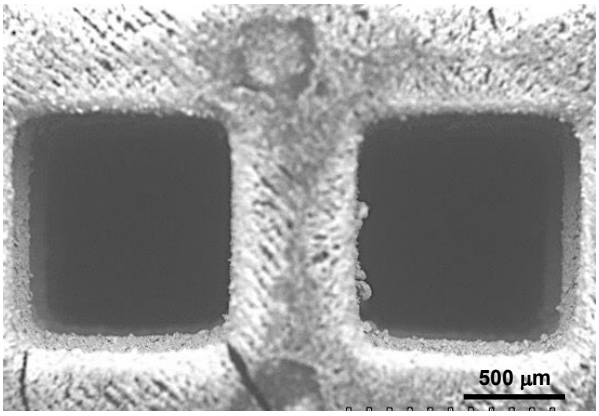

Figure 6. SEM image of the cross section of the AD monolith after a thermal treatment in air.

Chemical mapping of Ce confirms that the catalyst active phase forms a uniform layer on the polymeric surface of the monolith channels (**Figure 7b**). No Ce is obtained inside the resin layer, which indicates that active phase does not diffuse into the polymeric walls and thus, all the active phase anchor is disposed on the external surface of the resin walls being accessible for the gas reactants. Regarding the Cu mapping (**Figure 7a**), note that copper is well-dispersed all along the CeO_2 surface providing an adequate distribution of active sites available for the reaction.

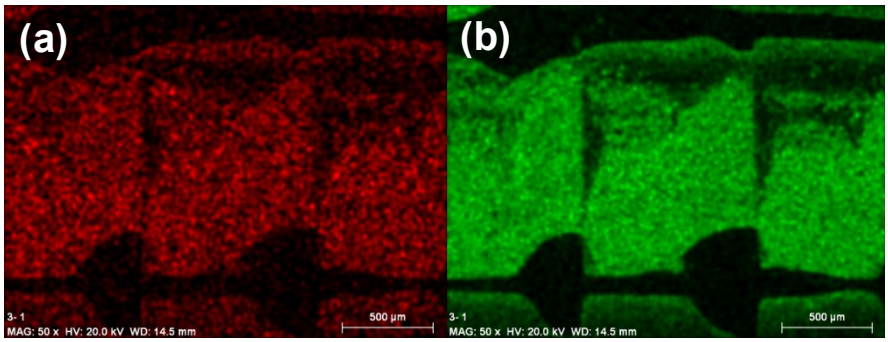

Figure 7. Chemical mapping of the CuO/CeO_2 catalyst deposited in the monolith channels with advanced design, (a) Cu and (b) Ce.

The powdered and supported active phase were also characterized by XRD, and the diffractograms are included in **Figure 8** along with pure CeO_2 used as reference. For the XRD characterization of supported catalysts, the monoliths were carefully slashed, and the X-Ray spot was focused on the surface of the active phase layer. It is important to highlight than the intensity of the peaks for the three supported samples can be affected by the background noise caused by the monolithic support and the dilution effect thereof. Comparing the different monoliths, it is observed that the peaks intensity is lower in the case of the CuO/CeO_2 supported on AD monolith after the treatment in N_2, CuO/CeO_2-AD (N_2), in which, as was observed from SEM images, a large part of the active phase was coated or embedded in the polymeric matrix. However, this intensity increases after

the air treatment, CuO/CeO_2-AD (air), reflecting in some way the elimination of the resin that could remain covering the surface and thus, increasing the accessibility to the CuO/CeO_2 active phase. Moreover, no changes in crystallinity are evident after the reaction.

Analyzing in more detail the X-ray diffractograms of all samples, characteristic peaks of the fluorite structure of ceria (JCPDS-340394) at 28.5, 33.1, 47.6, and 56.5 ° are observed, corresponding to the (111), (200), (220), and (311) planes, respectively. CuO peaks that could appear at 35.5° and 38.8° are not well defined, indicating that copper oxide is well dispersed on the ceria support forming small crystallites corroborating the observation obtained by Cu-mapping. Note that CeO_2 peaks are slightly displaced for CuO/CeO_2 catalyst regarding CeO_2 support, which is attributed to a structure distortion of ceria crystalline structure due to the insertion of Cu^{2+} cations into the ceria lattice. The lattice parameters of CeO_2 (0.5420 nm) is consistent with the value reported for ceria in the JCPDS 00-034-0394 reference database, and this value slightly decreased upon copper impregnation both for powdered and supported CuO/CeO_2 catalysts (0.5415 nm) which corroborates the insertion of copper cations into the ceria lattice.

The crystallite size of ceria was determined using the Scherrer equation. The crystallite sizes of the ceria fluorite phase are quite similar for powdered and supported active phase (8 nm), and closed to the value obtained for pure ceria (9 nm) which evidences that the incorporation of copper to the ceria does not affect the average size of the CeO_2 crystals.

Thus, XRD diffractograms reveals that there are not relevant differences in the crystalline phase supported on the 3D-printed monolith regarding the powdered catalyst.

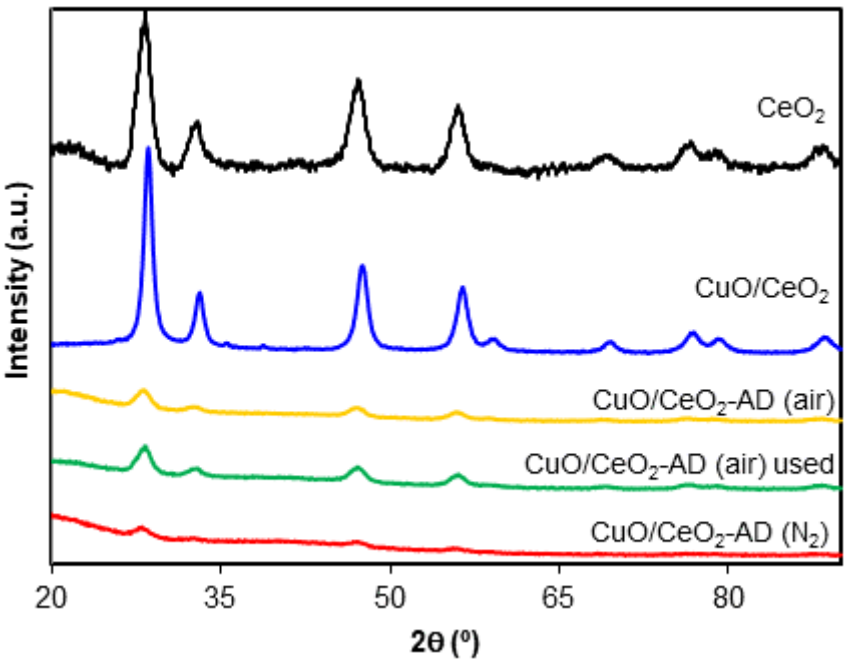

Figure 8. XRD diffractograms of CeO_2 and the CuO/CeO_2 catalyst, both powdered and supported (CuO/CeO_2-AD)

The same conclusions were obtained from Raman spectra of the active phases, which are included in **Figure 9**. A single band at 463.9 cm^{-1} is obtained for pure CeO_2, which is assigned to the F_{2g} mode of the fluorite structure of ceria. This peak is related to the vibration mode of the oxide anions around its equilibrium position in the octahedral sites of the cubic cell. A displacement of the F_{2g} peak to 455.0 cm^{-1} is obtained for the CuO/CeO_2 active phase, which is related to the presence of doping cations in the CeO_2 lattice, as it was already pointed out by XRD. In addition, a slight shoulder is detected in the spectra of the powdered and supported CuO/CeO_2 catalyst between 500 and 650 cm^{-1}, which is related to the presence of oxygen vacancies as a consequence of the incorporation of Cu^{2+} in the fluorite lattice. The observation of this band can be difficult at a relatively low concentration of oxygen vacancies. So, the evidence of these changes can be provided by the displacement and the width increase of the main Raman band of the F_{2g} mode, given that these parameters are much more sensitive to changes in the physical-chemical characteristics of the solids than the intensity of the bands, which is

affected by other variables such as the size of the crystal or the absorption of the radiation.[25–28]

On the other hand, the position of the F_{2g} peak is the same for the supported active phase on the 3D-printed monoliths regarding powdered active phase that confirms again that the ceria lattice is not modified by its deposition on the monoliths. However, the different accessibility of the active phase after both treatments was also pointed out by Raman. The intensity of the Raman signal after the thermal stabilization treatment under N_2 is practically negligible due to the incrustation or covering of the active phase by the resin, whereas this intensity strongly increases after the oxidation thermal treatment because of the removal of this surface resin deposits.

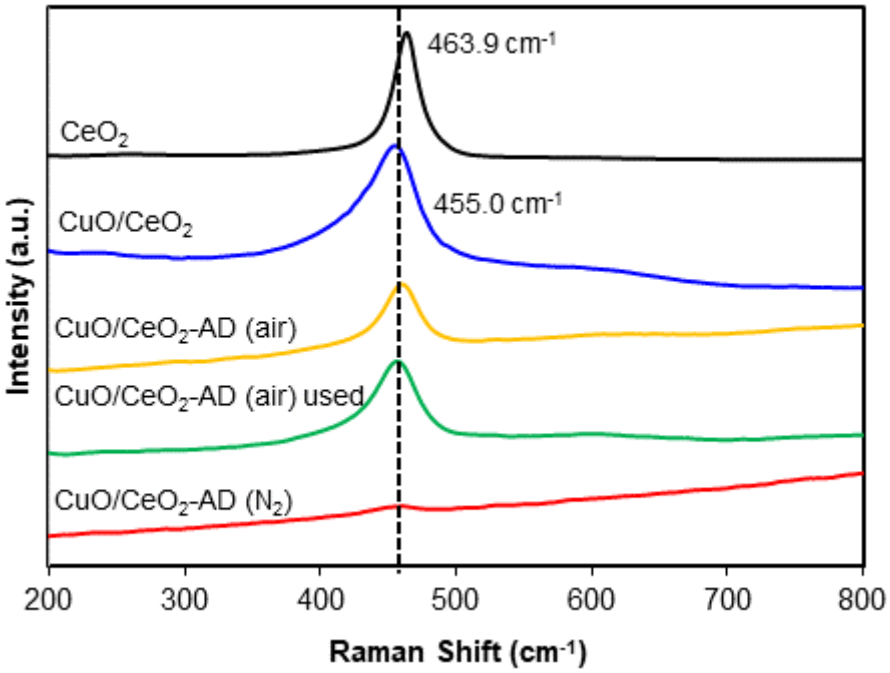

Figure 9. Raman spectra of CeO_2 and the CuO/CeO_2 catalyst, both powdered and supported (CuO/CeO_2-AD).

The surface of the powdered and supported on the 3D-printed monolith active phases was also analysed by XPS. Ce3d and Cu2p spectral regions are depicted in **Figure 10.** The $Cu2p_{3/2}$ region shows two contributions at 935.7 and 933.3 eV which can be assigned to

copper oxidized species with different electronic environment. The presence of the shake-up satellite peaks between 937-947 eV confirms the presence of Cu^{2+} cations. The Cu LMM Auger transition (Fig. 10c) is centered at about 916.7 eV, which also supports the lone presence of Cu^{2+} species. Regarding Ce3d regions, Ce^{3+} and Ce^{4+} species is detected, however the Ce^{3+} percentage is similar for supported and powdered active phases (18 %). Therefore, from XPS results it can be concluded that the surface chemistry of the powdered active phase is not extremely modified upon the deposition process and the resin does not affects the chemical nature of the CuO/CeO_2 active phase.

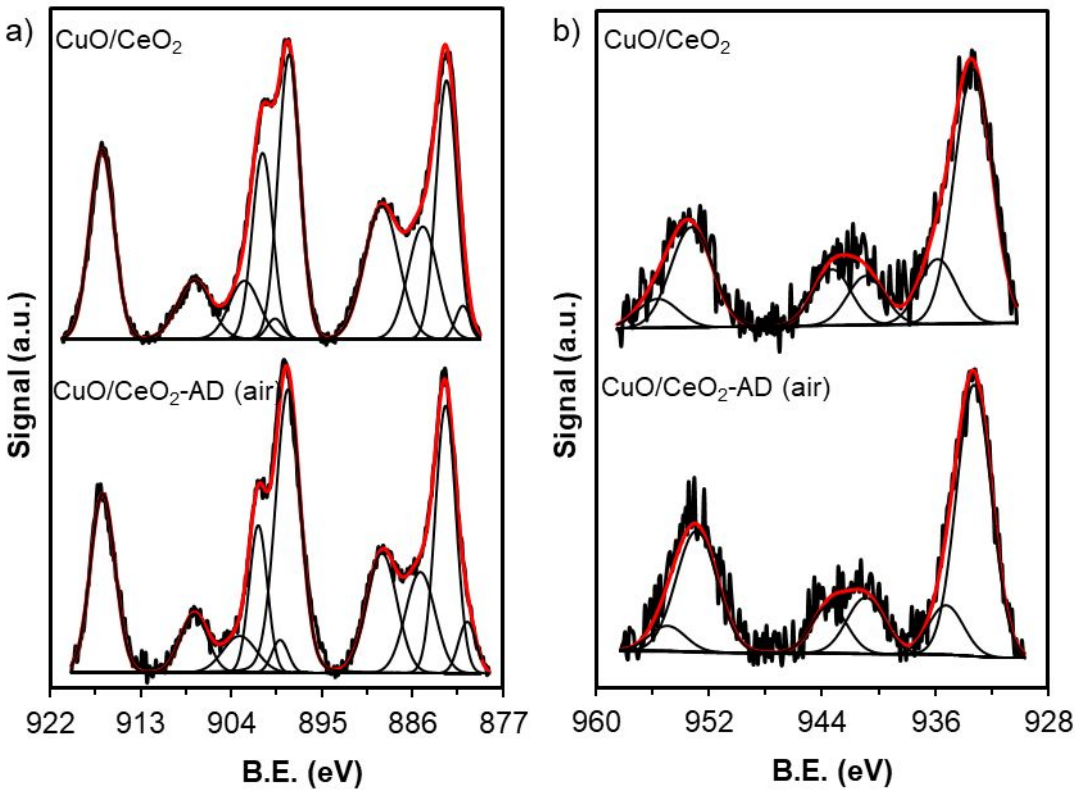

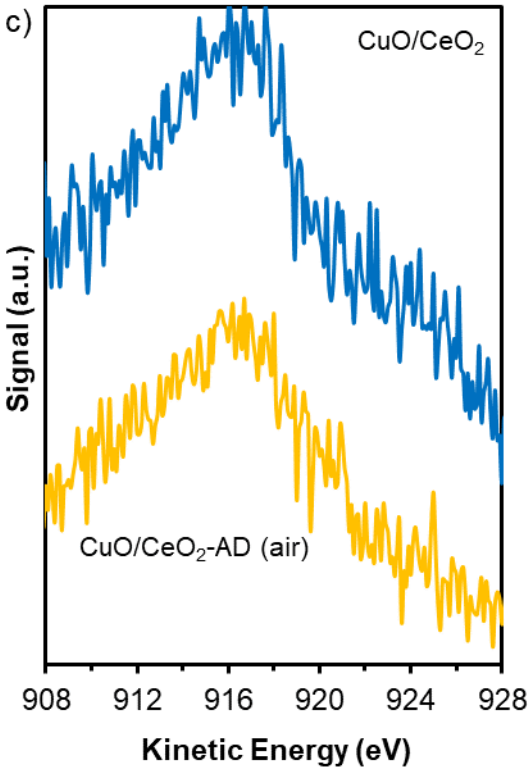

Figure 10. XPS characterization of the surface of powdered and supported active phase. (a) Ce3d, (b) Cu2p regions and (c) Cu LMM Auger range.

3.2. Characterization of the catalytic performance: CO oxidation in CO-PrOx conditions

CO oxidation in CO-PrOx conditions was performed under 2% CO, 2% O_2, 30% H_2 in He balance and a total flow of 30 ml/min, and the CO conversion and selectivity obtained for the powdered active phase and the monolithic-supported one after both air and N_2 thermal treatment are shown in **Figure 11.** The CuO/CeO_2 active phase is highly active and selective to the CO oxidation in presence of H_2. Total conversion is obtained at 125 ºC being completely selective to the CO oxidation regarding the H_2 one, and above this temperature, as expected, CO selectivity decreases due to the oxidation of H_2. Regarding the supported active phase, strong differences are observed depending on the thermal treatment. No activity is obtained after a thermal treatment in N_2, which

corroborates the observations obtained from the characterization. Most of the active phase is embedded or covered by the resin being not accessible to the reactants. However, after the oxidation treatment in air, the activity of the CuO/CeO_2 active phase is almost recovered due to the cleaning of the active phase surface (**Figure 5**) obtaining the maximum conversion of CO (97 %) at 150 ºC. This lower conversion obtained with the monolith (97 %) regarding the powdered active phase (99.8 %) can be explained on the base of radial mass diffusions problems caused by the laminar regime imposed by the gas diffusion thorough the straight channels. In addition, a temperature delay of 25 ºC is obtained for the supported active phase regarding the powdered one despite that, as it was pointed out in the characterization section, the active phases present identical properties in terms of crystallinity and surface chemistry. This delay can be attributed to the fact that part of the active phase remains inaccessible after oxidizing treatment, since the catalytic activity was compared at equal amount of active phase (51 mg of both powder or supported active phase) and gas hourly space velocity (GHSV) and consequently in the monolith, part of this active phase can still be covered by resin deposits. This has been confirmed performing several consecutive reaction cycles.

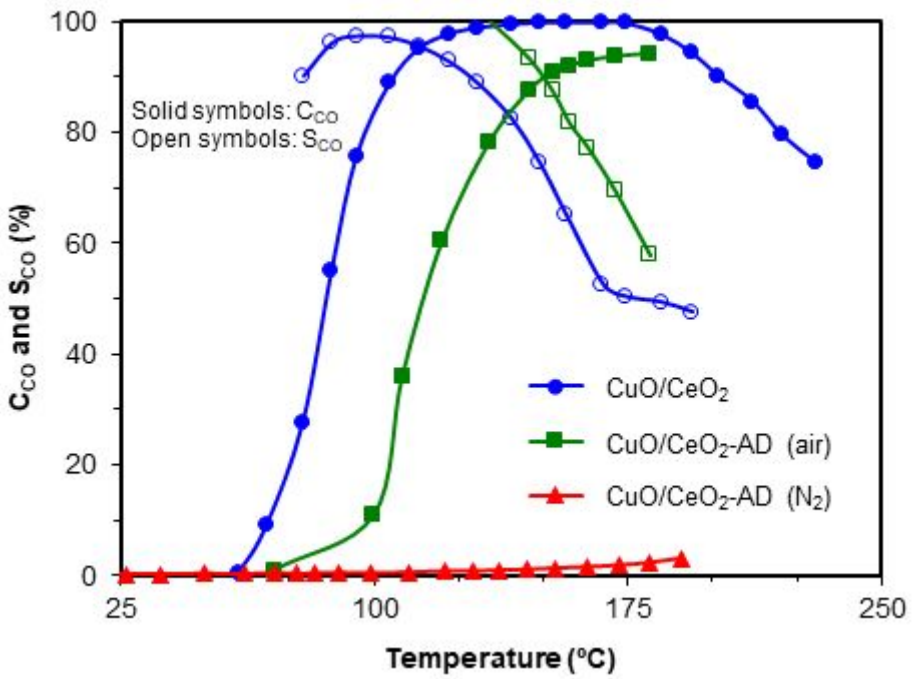

Figure 11. Conversion of CO (C_{CO}) and selectivity to the CO oxidation (S_{CO}) of the monolith thermally treated in N_2 (▲), monolith thermally treated in air (■) and CuO/CeO_2 active phase powder (●) for CO oxidation in CO-PROX conditions: 2% CO, 2% O_2, 30% H_2 in He balance and a total flow of 30 ml/min

Several reaction cycles were performed using the powdered (CuO/CeO_2) and supported active phases (CuO/CeO_2-AD air) and results are depicted in **Figure S1** and **12**. No changes in activity and selectivity are obtained after four reuse cycles for the powdered catalyst manifesting that, after the oxidation cooling process, the active phase has been easily regenerated demonstrating good stability and high reusability and recyclability. Regarding the supported active phase, an improvement in conversion is obtained after each reutilization cycle which corroborates the fact that part of the active phase is still inaccessible to the reactants as was also pointed out by XRD and Raman where an increase of the peak intensity is observed for the used monolithic catalysts (**Figure 8** and **9**). It is important to highlight that after 4 reuse cycles the activity of the active phase is almost recovered as it was pointed out in **Figure 12** where the temperature

required to achieve the 50 % of conversion is depicted as a function of the number of reuse cycles.

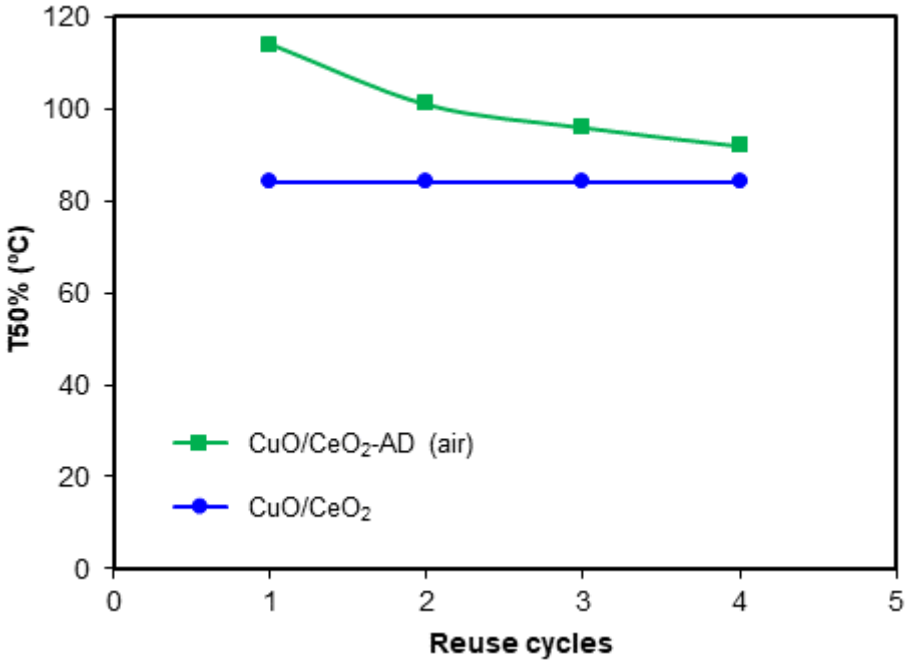

Figure 12. Study of the stability of the catalysts after being reused in successive cycles (flow of 30 ml/min).

The flow regime of the gas (laminar or turbulent) is a factor that influences the results obtained, since this regime can be different in the powder bed with respect to the monolith. In monoliths with straight channel, even for turbulent gases conditions, this flow becomes laminar when flowing inside the channel as a result of viscous forces inside the narrow channels,[29] hindering the radial diffusion of the reactants and thus, their accessibility to the active phase. In a powder bed, despite a turbulent regime predominates, laminar regime may occur by the generation of preferential paths that lead to the reaction proceeding under diffusional speed control. To analyze the effect of external mass diffusion on the reaction rate, catalytic tests were performed at different gas flow rates (from 30 to 120 ml/min) and results are shown in **Figure 13.** Both powdered and supported active phases work under diffusional control at a flow of 30

ml/min above which chemical control is achieved. However, by increasing the gas flow rate to 90 ml/min, the reaction rate of the powdered catalyst remains under chemical control to about 68 °C, while the reaction rate of the supported catalyst (monolith) is still under chemical control up to about 80 ºC. This manifests that the deposition of the active phase in the monolith significantly affects the rate control regime. At higher flow (120 ml/min), chemical control is maintained up to higher temperature (85-90 ºC) in both cases, however, in the monolith a temperature displacement of the curve at around 4 ºC is observed which can be related with heat diffusion problems imposed by the radial heat dispersion inside straight channels. CO-PrOx is a highly exothermic reaction and the generated heat flow must be dispersed mainly by the gas flow. At low flow rates, the net heat generated (KJ/mol) is low enough to be dispersed by convection into the mass flow, and thus, the real temperature in the active site is similar to the measured one. However, at high flow rates (120 ml/min), the net heat generated is so high and a local increase of the temperature is obtained in the active sites and thus, the temperature at the active site is higher than the measured one with the corresponding increase of the conversion. In the powdered catalysts, the turbulent flow created through the catalytic bed and the use of SiC favors the heat transfers avoiding this local temperature increase.

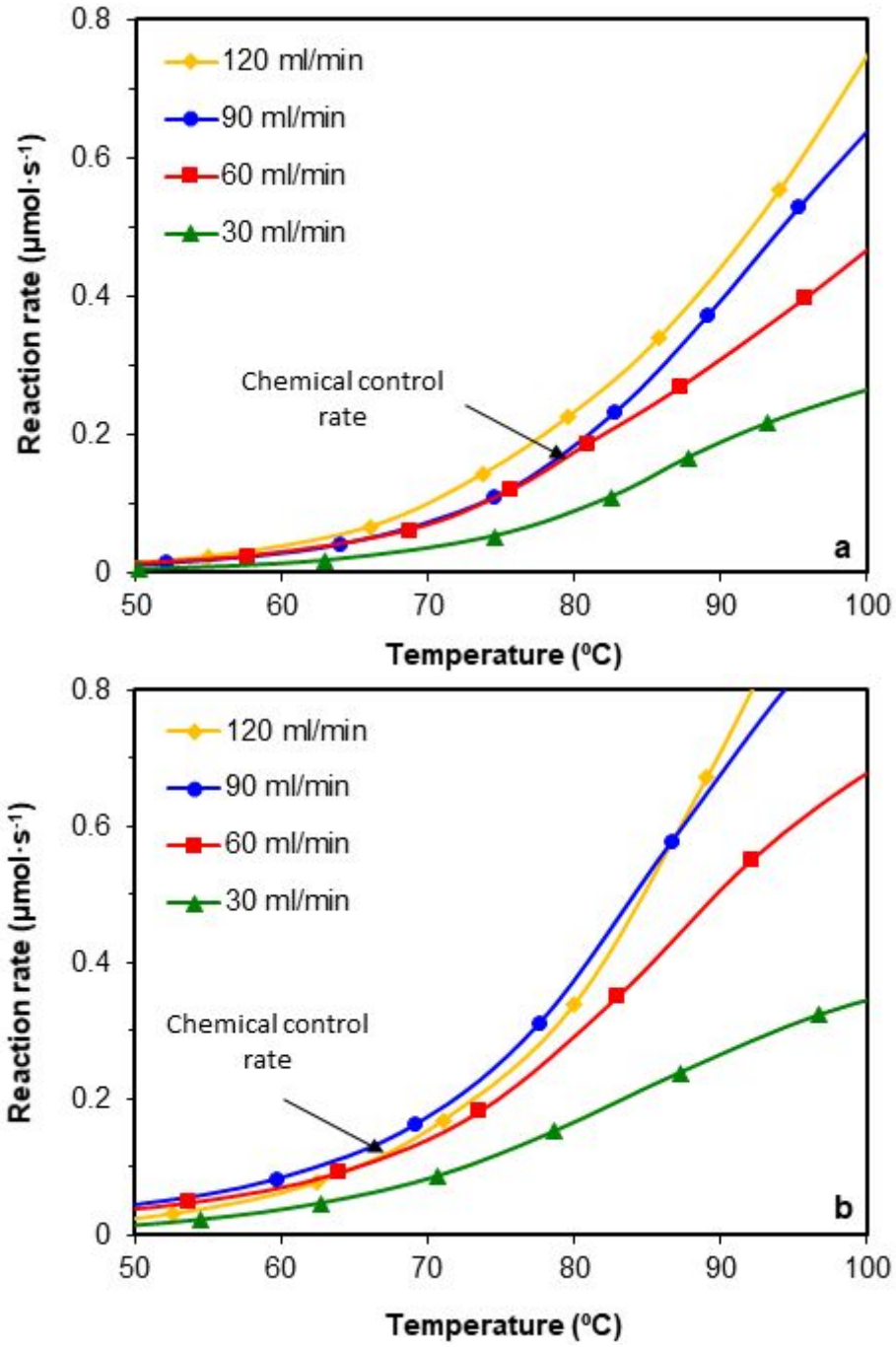

Figure 13. Oxidation rate of CO in CO-PrOx experiments carried out with the supported catalyst in the monolith (a) and the powder catalyst (b).

Finally, to complete the catalytic study, a stability test to the supported catalyst (**Figure 14**) was performed for 10 hours with a flow of 60 ml/min and at constant temperature (135 ° C). Both CO conversion (95%) and CO selectivity (90%) remain stable in this time range, demonstrating a good catalytic activity for long reaction times.

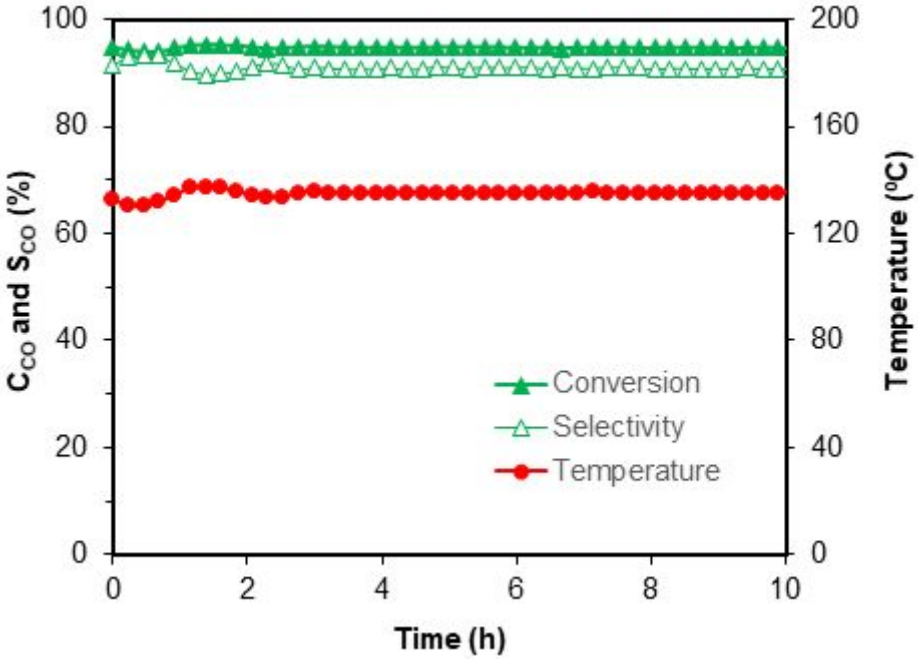

Figure 14. CO conversion (C_{CO}) and selectivity to CO oxidation (S_{CO}) (in the main axis) and temperature (in the secondary axis) for the CuO/CeO_2-AD (air) catalyst. Reaction conditions: 2% O_2, 2% CO, 30% H_2 and, and He balance. Total flow of 60 ml/min at constant temperature

Briefly, the supported catalyst exhibited good catalytic activity, although the conversion obtained is slightly lower than the expected conversions for the powdered CuO/CeO_2 catalyst. This result has been influenced by effects of the catalyst-polymer resin interaction, as well as the mass diffusional restrictions imposed by the geometry of the monolithic support. Once overcome the difficulties to anchor active phases on polymeric supports and taking into account the results obtained in this work, the gate is open to obtain monoliths with improved catalytic behavior. Therefore, considering the advantages of the 3D-printing technology, advanced monoliths with more complex structures can be obtained by introduction of modifications in the geometry that break the laminar flow imposed by the straight channel of conventional monolithic supports.

4. Conclusions

Polymeric monoliths were obtained by 3D-printing and successfully tested as supports of CuO/CeO_2 active phase in the reaction of preferential oxidation of CO (CO-PrOx). Different strategies were performed in order to overcome the handicap of the active phase incorporation to the polymeric support, such as addition of inorganic materials (carbon or silica) to the polymer previous to the printing process, chemical attack of the printed resin previous or during the active phase incorporation, perform consecutives impregnations or modification of the channel walls design. From all the above results and discussion, the following conclusions can be drawn:

i) It has been possible to identify that the addition of several charges of carbon or silica in the resin composition does not promote changes in its thermal stability, but it improves the amount of active phase anchored to the monoliths.

ii) A greater amount of active phase was anchored in the monoliths printed with the advanced design (channel walls with prismatic cavities) regarding the conventional design (flat walls). The optimal monoliths to support the active phase were those that were printed with advanced design from pure resin, since they allowed anchoring a significant amount of active phase in a single impregnation step.

iii) The stabilization thermal treatment of the impregnated monolith was defined as a fundamental step to soften the resin and favor the active phase anchoring. However, catalyst particles become embedded on the polymeric resin being not active and thus, a final cleaning thermal treatment under air was needed to recover the active phase activity, after which the supported active phase showed good activity, stability and high reusability.

iv) The supported CuO/CeO_2 catalyst presented a catalytic activity slightly lower than that of the powder active phase for the CO-PrOx reaction, however after several reuse cycles, the activity of the supported catalyst is enhanced and thus, the polymeric supports are considered a viable alternative for application in PEMFCs due to the advantages of the monolithic supports with respect to powdered catalysts.

v) According to the results obtained in this study and the good performance in the CO-PrOx reaction presented by the CuO/CeO_2 catalyst supported in polymer resin monoliths, the role played by 3D printing to obtain catalyst supports is highlighted. This opens the gate to the design and manufacture of monolithic supports with complex structures, which will allow to optimize the catalysts by means of changes in the geometry of the monoliths.

5. Acknowledgements

The authors thank the financial support of the Spanish Ministry of Economy and Competitiveness (Project CTQ2015-67597-C2-2-R and grant FJCI-2015-23769), the Spanish Ministry of Education, Culture and Sports (grant FPU14/01178), Generalitat Valenciana (Project PROMETEO/2018/076 and PhD grant GRISOLIAP/2017/177) and the UE (FEDER funding).

6. Supporting Information

Reuse of the powdered and the monoliths-supported catalyst.

7. References

(1) Dincer, I.; Acar, C. Review and Evaluation of Hydrogen Production Methods for Better Sustainability. *Int. J. Hydrogen Energy* **2014**, *40* (34), 11094–11111.

(2) Acar, C.; Dincer, I. Comparative Assessment of Hydrogen Production Methods from Renewable and Non-Renewable Sources. *Int. J. Hydrogen Energy* **2014**, *39* (1), 1–12.

(3) Armor, J. N. The Multiple Roles for Catalysis in the Production of H_2. *Appl. Catal. A Gen.* **1999**, *176* (2), 159–176.

(4) Dincer, I. Green Methods for Hydrogen Production. *Int. J. Hydrogen Energy* **2012**, *37* (2), 1954–1971.

(5) Yang, H.; Xu, Z.; Fan, M.; Gupta, R.; Slimane, R. B.; Bland, A. E.; Wright, I. Progress in Carbon Dioxide Separation and Capture: A Review. *J. Environ. Sci.* **2008**, *20* (1), 14–27.

(6) Bion, N.; Epron, F.; Moreno, M.; Mariño, F.; Duprez, D. Preferential Oxidation of Carbon Monoxide in the Presence of Hydrogen (PROX) over Noble Metals and Transition Metal Oxides: Advantages and Drawbacks. *Top. Catal.* **2008**, *51* (1–4), 76–88.

(7) Choudhary, T. CO-Free Fuel Processing for Fuel Cell Applications. *Catal. Today* **2002**, *77* (1–2), 65–78.

(8) Farrauto, R.; Hwang, S.; Shore, L.; Ruettinger, W.; Lampert, J.; Giroux, T.; Liu, Y.; Ilinich, O. New Material Needs for Hydrocarbon Fuel Processing: Generating Hydrogen for the PEM Fuel Cell. *Annu. Rev. Mater. Res.* **2003**, *33* (1), 1–27.

(9) Ghenciu, A. F. Review of Fuel Processing Catalysts for Hydrogen Production in PEM Fuel Cell Systems. *Curr. Opin. Solid State Mater. Sci.* **2002**, *6* (5), 389–399.

(10) Park, E. D.; Lee, D.; Lee, H. C. Recent Progress in Selective CO Removal in a H_2-Rich Stream. *Catal. Today* **2009**, *139* (4), 280–290.

(11) Reshetenko, T. V.; Bethune, K.; Rubio, M. A.; Rocheleau, R. Study of Low Concentration CO Poisoning of Pt Anode in a Proton Exchange Membrane Fuel Cell Using Spatial Electrochemical Impedance Spectroscopy. *J. Power Sources* **2014**, *269*, 344–362.

(12) Barbato, P. S.; Di Benedetto, A.; Landi, G.; Lisi, L. CuO/CeO_2 Based Monoliths for CO Preferential Oxidation in H2-Rich Streams. *Chem. Eng. J.* **2015**, *279*, 983–993.

(13) Zeng, S.; Zhang, W.; Śliwa, M.; Su, H. Comparative Study of CeO_2/CuO and CuO/CeO_2 Catalysts on Catalytic Performance for Preferential CO Oxidation. *Int. J. Hydrogen Energy* **2013**, *38* (9), 3597–3605.

(14) Zhang, Q.; Shore, L.; Farrauto, R. J. Selective CO Oxidation over a Commercial PROX Monolith Catalyst for Hydrogen Fuel Cell Applications. *Int. J. Hydrogen Energy* **2012**, *37* (14), 10874–10880.

(15) Reina, T. R.; Papadopoulou, E.; Palma, S.; Ivanova, S.; Centeno, M. A.; Ioannides, T.; Odriozola, J. A. Could an Efficient WGS Catalyst Be Useful in the CO-PrOx Reaction? *Appl. Catal. B Environ.* **2014**, *150–151*, 554–563.

(16) Landi, G.; Barbato, P. S.; Di Benedetto, A.; Lisi, L. Optimization of the Preparation Method of CuO/CeO_2 Structured Catalytic Monolith for CO Preferential Oxidation in H_2-Rich Streams. *Appl. Catal. B Environ.* **2016**, *181*, 727–737.

(17) Barbato, P. S.; Di Benedetto, A.; Landi, G.; Lisi, L. Structuring CuO/CeO_2 Catalyst as Option to Improve Performance Towards CO-PROX. *Top. Catal.* **2016**, *59* (15–16), 1371–1382.

(18) Avila, P.; Montes, M.; Miró, E. E. Monolithic Reactors for Environmental Applications: A Review on Preparation Technologies. *Chem. Eng. J.* **2005**, *109*

(1), 11–36.

(19) Cybulski, A.; Moulin, J. Monoliths in Heterogeneous Catalysis. *Catal. Rev.* **1994**, *36* (2), 179–270.

(20) Govender, S.; Friedrich, H. Monoliths: A Review of the Basics, Preparation Methods and Their Relevance to Oxidation. *Catalysts* **2017**, *7* (12), 62.

(21) Williams, J. L. Monolith Structures, Materials, Properties and Uses. *Catal. Today* **2001**, *69*, 3–9.

(22) Boger, T.; Heibel, A. K.; Sorensen, C. M. Monolithic Catalysts for the Chemical Industry. *Ind. Eng. Chem. Res.* **2004**, *43* (16), 4602–4611.

(23) González-Velasco, J. R.; Gutiérrez-Ortiz, M. A.; Ferret, R.; Aranzabal, A.; Botas, J. A. Synthesis of Cordierite Monolithic Honeycomb by Solid State Reaction. *J. Mater. Sci.* **1999**, *4* (34), 1999–2002.

(24) Balan, L.; Fernández de Córdoba, M. C.; Zaier, M.; Ania, C. O. A Green and Fast Approach to Nanoporous Carbons with Tuned Porosity: UV-Assisted Condensation of Organic Compounds at Room Temperature. *Carbon N. Y.* **2017**, *116*, 264–274.

(25) Guillén-Hurtado, N.; Bueno-López, A.; García-García, A. Surface and Structural Characterisation of Coprecipitated $Ce_xZr_{1-x}O_2$ ($0 \geq x \geq 1$) Mixed Oxides. *J. Mater. Sci.* **2012**, *47* (7), 3204–3213.

(26) Rico-Pérez, V.; Aneggi, E.; Bueno-López, A.; Trovarelli, A. Synergic Effect of $Cu/Ce_{0.5}Pr_{0.5}O2_{-\delta}$ and $Ce_{0.5}Pr_{0.5}O_{2-\delta}$ in Soot Combustion. *Appl. Catal. B Environ.* **2016**, *197*, 95–104.

(27) Gamarra, D.; Cámara, A. L.; Monte, M.; Rasmussen, S. B.; Chinchilla, L. E.; Hungría, A. B.; Munuera, G.; Gyorffy, N.; Schay, Z.; Corberán, V. C.; Conesa, J.C.; Martínez-Arias, A. Preferential Oxidation of CO in Excess H_2 over CuO/CeO_2 Catalysts: Characterization and Performance as a Function of the Exposed Face Present in the CeO_2 Support. *Appl. Catal. B Environ.* **2013**, *130–131*, 224–238.

(28) Davó-Quiñonero, A.; Navlani-García, M.; Lozano-Castelló, D.; Bueno-López, A.; Anderson, J. A. Role of Hydroxyl Groups in the Preferential Oxidation of CO over Copper Oxide-Cerium Oxide Catalysts. *ACS Catal.* **2016**, *6* (3), 1723–1731.

(29) Mu, M.; Sjöblom, J.; Ström, H.; Li, X. Analysis of the Flow Field from Connection Cones to Monolith Reactors. *Energies* **2019**, *12* (3), 455.

Table of Content